Triangular flow in heavy ion collisions in a multiphase transport model

Jun Xu[1] and Che Ming Ko[2]

[1]*Cyclotron Institute, Texas A&M University, College Station, TX 77843-3366, USA*
[2]*Cyclotron Institute and Department of Physics and Astronomy, Texas A&M University, College Station, TX 77843-3366, USA*

(Dated: February 16, 2022)

We have obtained a new set of parameters in a multiphase transport (AMPT) model that are able to describe both the charged particle multiplicity density and elliptic flow measured in Au+Au collisions at center of mass energy $\sqrt{s_{NN}} = 200$ GeV at the Relativistic Heavy Ion Collider (RHIC), although they still give somewhat softer transverse momentum spectra. We then use the model to predict the triangular flow due to fluctuations in the initial collision geometry and study its effect relative to those from other harmonic components of anisotropic flows on the di-hadron azimuthal correlations in both central and mid-central collisions.

PACS numbers: 25.75.-q, 12.38.Mh, 24.10.Lx

arXiv:1103.5187v3 [nucl-th] 28 Jun 2011

I. INTRODUCTION

Studies of anisotropic azimuthal flows in heavy ion collisions at RHIC have provided important information on the properties of produced quark-gluon plasma (QGP) [1–4]. In particular, the large elliptic flow observed in experiments has led to the conclusion that the produced quark-gluon plasma is strongly interacting as it can only be explained in the hydrodynamic model with a very small viscosity [5–8] or in the transport model with parton scattering cross sections much larger than those given by the perturbative QCD [9, 10]. With the large parton scattering cross section, the transport model has also been able to describe the hexadecupole flow measured at RHIC [11]. More recently, the importance of the triangular flow, which originates from fluctuations in the initial collision geometry [12], has been pointed out in Ref. [13]. Unlike the elliptic flow, the triangular flow is less sensitive to the centrality or the impact parameter of the collision [13–15]. Also, a study based on the viscous hydrodynamics has shown that the viscosity in the quark-gluon plasma has a larger effect on the triangular flow than the elliptic flow in relativistic heavy ion collisions [16]. Furthermore, it was suggested in Ref. [13] and later shown in Ref. [17] in a multiphase transport (AMPT) model, which includes both initial partonic and final hadronic scatterings, that the triangular flow may play an important role in the away-side double-peak structure seen in the di-hadron azimuthal correlations at RHIC. In the present paper, we extend the study of Ref. [17] to investigate more quantitatively the triangular flow in heavy ion collisions at RHIC by adjusting the parameters in the AMPT model, particularly the parton scattering cross section, to fit more recent experimental data such as the charged particle multiplicity density and transverse momentum spectra as well as their elliptic flow. We find that the resulting triangular flow has smaller values than those shown in Ref. [17] but still has an appreciable effect on the di-hadron azimuthal correlations as found in Ref. [17].

This paper is organized as follows. In Sec. II, we review the AMPT model and discuss the parameters in the model that are relevant to the present study. In Sec. III, we describe the results on the charged particle multiplicity density and transverse momentum spectra in heavy ion collisions at RHIC and their comparisons with experimental data. We then show in Sec. IV the calculated charged particle elliptic flow in comparison with the experimental measurements as well as the predicted triangular flow. In Sec. V, we study the effect of anisotropic flows, particularly that of triangular flow, on the di-hadron azimuthal correlations. In Sec. VI, we discuss the specific viscosity in the initial partonic matter produced in heavy ion collisions. Finally, a summary is given in Sec. VII.

II. THE AMPT MODEL

The AMPT model is a hybrid model [18] with the initial particle distributions generated by the heavy ion jet interaction generator (HIJING) model [19]. In the default version, the jet quenching in the HIJING model is replaced in the AMPT model by explicitly taking into account the scattering of mini-jet partons via the Zhang's parton cascade (ZPC) model [20]. These partons are recombined with their parent strings after the scattering, which are then converted to hadrons using the Lund string fragmentation model. In the version of string melting, all hadrons produced from the string fragmentation in the HIJING model are converted to their valence quarks and antiquarks, whose evolution in time and space is modeled by the ZPC model. After the end of their scatterings, quarks and aniquarks are converted to hadrons via a spatial coalescence model. In both versions of the AMPT model, the scatterings among hadrons are described by a relativistic transport (ART) model [21].

In previous studies, it was found that the multiplicity of charged particles measured in heavy ion collisions at RHIC could be well described by the default AMPT model with modified values of a and b [22] in the Lund string fragmentation function $f(z) \propto z^{-1}(1 -$

TABLE I: Values of parameters for the Lund string fragmentation and the parton scattering cross section in previous studies (A) and in the present work (B).

	a	b (GeV^{-2})	α_s	μ (fm^{-1})
A	2.2	0.5	0.47	1.8
B	0.5	0.9	0.33	3.2

$z)^a \exp(-b\ m_\perp^2/z)$, where z is the light-cone momentum fraction of the produced hadron of transverse mass $m_\perp$ with respect to that of the fragmenting string. To describe the measured elliptic flow required, on the other hand, the AMPT model with string melting together with a larger parton scattering cross section $\sigma \approx 9\pi\alpha_s^2/(2\mu^2)$, where α_s is the QCD coupling constant and μ is the screening mass of a gluon in the QGP, than that given in the perturbative QCD. Values for these parameters are given in the first row (A) of Table I. In these studies [11, 23], the elliptic flow was calculated with respect to the theoretical reaction plane, corresponding to the second-order event plane $\Psi_2 = 0$. As a result, this might have underestimated the elliptic flow that is determined with non-zero Ψ_2 to take into account the fluctuations in the initial collision geometry as in the experimental analysis. We have recently shown, however, that both the charged particle multiplicity density and elliptic flow measured in heavy ion collisions at the Large Hadron Collider (LHC) can be described by the AMPT model with string melting by using the default a and b parameters in the HIJING model together with a smaller QCD coupling constant and a larger screening mass as given in the second row (B) in Table I [24]. We note that the parton scattering cross sections for parameter sets A and B are about 10 mb and 1.5 mb, respectively. Although the latter has a smaller value, it has a more isotropic angular distribution.

III. CHARGED PARTICLE MULTIPLICITY DENSITY AND TRANSVERSE MOMENTUM SPECTRA AT RHIC

We first show in Fig. 1 the centrality dependence of the multiplicity density of mid-pseudorapidity charged particles in Au+Au collisions at $\sqrt{s_{NN}} = 200$ GeV obtained from the AMPT model with string melting for the two parameter sets in Table I and compare them with the experimental data from the BRAHMS Collaboration [25]. For the relation between the centrality c and the impact parameter b, we use the empirical formula $c = \pi b^2/\sigma_{\rm in}$ [26] with the nucleus-nucleus total inelastic cross section $\sigma_{\rm in} \approx 705$ fm^2 calculated from the Glauber model. It is seen that the multiplicity densities from the parameter set A shown by filled triangles are larger than the BRAHMS data shown by filled squares at all centrality bins, while those from the parameter set B, which are given by filled circles, are consistent with the BRAHMS data.

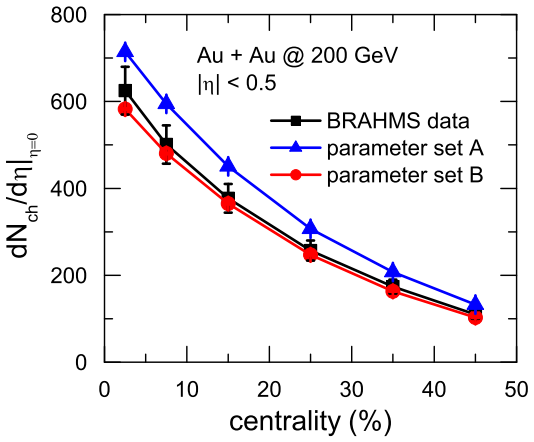


FIG. 1: (Color online) Centrality dependence of the multiplicity density of mid-pseudorapidity charged particles produced in Au+Au collisions at $\sqrt{s_{NN}} = 200$ GeV from the AMPT model with string melting using parameter sets A (filled triangles) and B (filled circles). The BRAHMS data shown by filled squares are from Ref. [25].

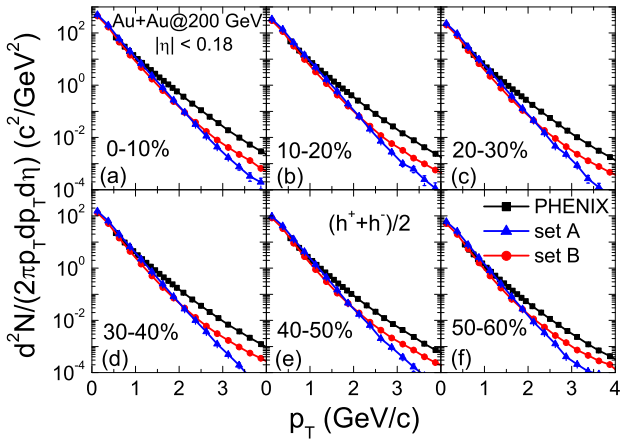


FIG. 2: (Color online) Transverse momentum spectra of mid-pseudorapidity ($|\eta| < 0.18$) charged particles by using parameter sets A (filled triangles) and B (filled circles) in Au+Au collisions at $\sqrt{s_{NN}} = 200$ GeV. The PHENIX data shown by filled squares are taken from Ref. [27].

Figure 2 shows the transverse momentum (p_T) spectra of mid-pseudorapidity charged particles in different centrality bins ($0-60\%$) from parameter sets A (filled triangles) and B (filled circles). It is seen that both parameter sets describe reasonably the experimental data from the PHENIX Collaboration [27] at low p_T. At high p_T, the parameter set B gives a larger yield than the parameter

set A as a result of smaller energy loss of high-p_T particles when the particle density is lower and the parton scattering cross section is smaller as for the parameter set B. As in the previous study [18], the p_T spectra from both parameter sets are softer than the experimental data, and this is due to the small current quark masses used in the AMPT model so that partons are less affected by the radial flow effect.

IV. CHARGED PARTICLE ANISOTROPIC FLOWS AT RHIC

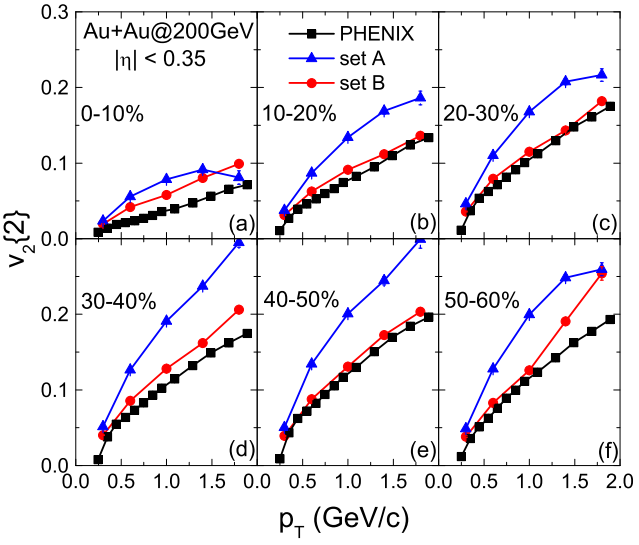


FIG. 3: (Color online) Transverse momentum dependence of the elliptic flow of mid-pseudorapidity ($|\eta| < 0.35$) charged particles by using parameter sets A (filled triangles) and B (filled circles) in Au+Au collisions at $\sqrt{s_{NN}} = 200$ GeV from the two-particle cumulant method. The PHENIX data shown by filled squares are taken from Ref. [28].

In Fig. 3, we compare the transverse momentum dependence of the elliptic flow of mid-pseudorapidity charged particles in different centrality bins $(0-60\%)$ of same collisions from the two parameter sets with the experimental data from the PHENIX Collaboration [28]. In both theoretical calculations and experimental analyses, the elliptic flow is determined using the two-particle cumulant method [29, 30]

$$v_2\{2\} = \sqrt{\langle \cos(2\Delta\phi) \rangle}, \tag{1}$$

where $\Delta\phi$ is the azimuthal angular difference between particle pairs within the same event and $\langle \cdots \rangle$ denotes average over all possible pairs. As the nonflow effect is overestimated at higher p_T in the AMPT model as shown in Ref. [24], we only compare the anisotropic flows at lower p_T where the nonflow effect is small. It is seen that for all centralities, the elliptic flow is larger for the parameter set A than for the parameter set B. This originates from two effects. First, the larger string tension in parameter set A leads to a larger number of initial particles, which results in a larger pressure and thus a larger anisotropic flow. Second and more importantly, the larger parton scattering cross section in parameter set A converts more efficiently the initial spatial anisotropy to the final momentum anisotropy. As for the charged particle multiplicity density and transverse momentum spectra, the parameter set B gives a much better description of the measured elliptic flow than the parameter set A.

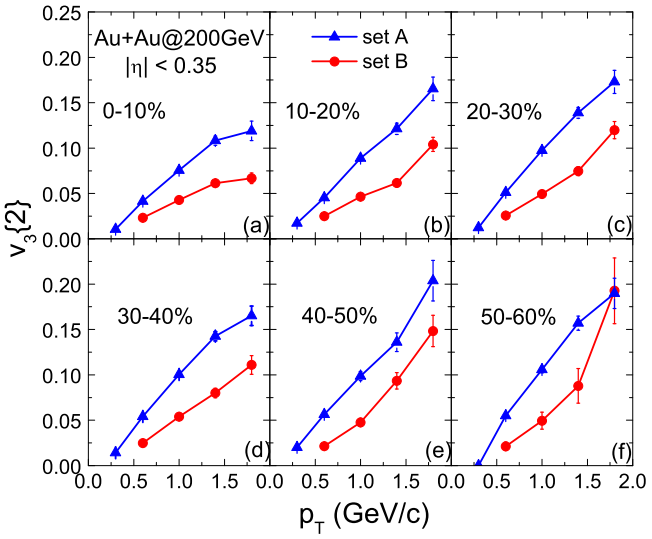


FIG. 4: (Color online) Transverse momentum dependence of the triangular flow of mid-pseudorapidity ($|\eta| < 0.35$) charged particles by using parameter sets A (filled triangles) and B (filled circles) in Au+Au collisions at $\sqrt{s_{NN}} = 200$ GeV from the two-particle cumulant method.

We have also studied the transverse momentum dependence of the triangular flow of mid-pseudorapidity charged particles in different centrality bins $(0-60\%)$ in Au+Au collisions at $\sqrt{s_{NN}} = 200$ GeV. Results obtained from the two-particle cumulant method, i.e., $v_3\{2\} = \sqrt{\langle \cos(3\Delta\phi) \rangle}$, are shown in Fig. 4 using both parameter sets A (filled triangles) and B (filled circles). Compared with the elliptic flow shown in Fig. 3, the triangular flow is smaller and less dependent on the centrality. Similar to the case of elliptic flow, the triangular flow is larger for the parameter set A than for the parameter set B. Since the parameter set B has been shown to give a better description of the charged particle multiplicity density, transverse momentum spectra, and elliptic flow, we believe that it would also give a more reliable prediction for the triangular flow. We note that the magnitude of the triangular flow from the parameter set B is

similar to that from the $(3+1)d$ viscous hydrodynamic model [16] with the specific viscosity of the value 0.08 and the transport+hydrodynamics hybrid approach [15] but a little larger than that in Ref. [13] based on the AMPT model.

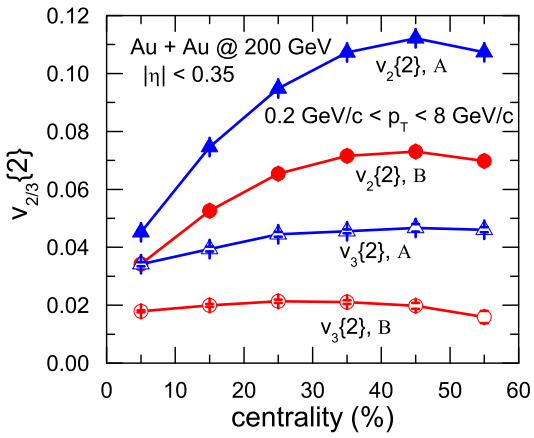


FIG. 5: (Color online) Centrality dependence of the elliptic flow (filled symbols) and the triangular flow (open symbols) from parameter sets A (triangles) and B (circles) in Au+Au collisions at $\sqrt{s_{NN}} = 200$ GeV for mid-pseudorapidity ($|\eta| < 0.35$) charged particles in the transverse momentum window 0.2 GeV/c $< p_T <$ 8 GeV/c from the two-particle cumulant method.

Figure 5 displays the centrality dependence of the elliptic flow (filled symbols) and the triangular flow (open symbols) of mid-pseudorapidity charged particles in the transverse momentum window 0.2 GeV/c $< p_T <$ 8.0 GeV/c from the two-particle cumulant method. Compared to the elliptic flow, the triangular flow shows a much weaker centrality dependence. As for the p_T-dependent differential flows, the momentum-integrated flows are larger for the parameter set A than for the parameter set B. Both elliptic and triangular flows increase with increasing centrality at small centralities but saturate or decrease at large centralities. Again, results from the parameter set B are similar to those from the transport+hydrodynamics hybrid approach [15].

V. DI-HADRON AZIMUTHAL CORRELATIONS

The effect of anisotropic flows on the di-hadron azimuthal correlations is a topic of great current interest [13, 17, 31–33] and can be studied by considering

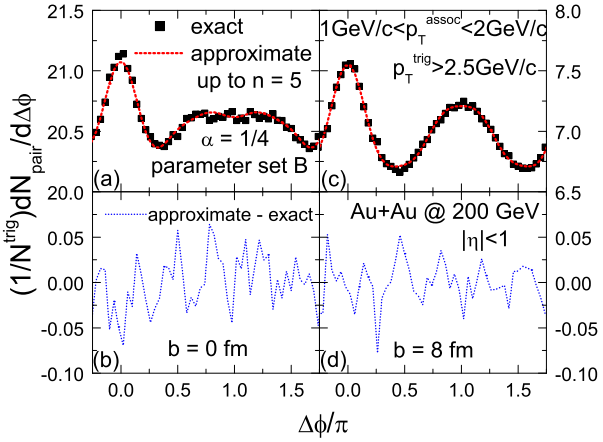


FIG. 6: (Color online) Comparison of the exact azimuthal correlations per trigger particle with the approximate ones defined in Eq. (2) up to order $n = 5$ in Au+Au collisions at $\sqrt{s_{NN}} = 200$ GeV for impact parameters b = 0 fm ((a) and (b)) and b = 8 fm ((c) and (d)) from the parameter set B.

following approximate azimuthal correlations:

$$\left\langle \frac{dN_{\rm pair}}{d\Delta\phi} \right\rangle_{\rm e} = \frac{1}{2\pi}[\langle N^{\rm trig} N^{\rm assoc}\rangle_{\rm e} + 2\sum_{n=1}^{+\infty}\langle N^{\rm trig} N^{\rm assoc} v_n^{\rm trig} v_n^{\rm assoc}\rangle_{\rm e}\cos(n\Delta\phi)], \quad (2)$$

where $\langle\cdots\rangle_{\rm e}$ denotes average over all events, $N^{\rm trig}$ and $N^{\rm assoc}$ are numbers of trigger and associated particles, and $v_n^{\rm trig}$ and $v_n^{\rm assoc}$ are, respectively, their nth-order anisotropic flows. The nth-order anisotropic flow is calculated with respect to the corresponding event plane defined by

$$\psi_n = \frac{1}{n}\arctan\frac{\langle p_T^\alpha \sin(n\phi)\rangle}{\langle p_T^\alpha \cos(n\phi)\rangle}, \quad (3)$$

where ϕ is the azimuthal angle and p_T^α is the weight factor. As in Ref. [31], we take the transverse momenta of trigger particles to be $p_T^{\rm trig} > 2.5$ GeV/c, corresponding mostly from the fragmentation of energetic jets produced in initial hard scatterings that have not interacted much with the produced medium. For the associated particles, their transverse momenta are taken in the window 1 GeV/$c < p_T^{\rm assoc} <$ 2 GeV/c as in Ref. [31], and they are medium particles after the passage of initially produced back-to-back jet pairs. At mid-pseudorapidity ($|\eta| < 1$), the numbers of trigger particles and associated particles from the AMPT model are, respectively, 1.336 and 128.6 for b = 0 fm, and 0.565 and 42.3 for b = 8 fm. We first show in the upper panels of Fig. 6 by filled squares the exact di-hadron azimuthal correlations per trigger particle calculated from all possible pairs of trigger particles

and associated particles from the AMPT model for the two impact parameters b = 0 fm and b = 8 fm, corresponding to central and mid-central collisions, respectively. It is seen that for both impact parameters there is a peak around $\Delta\phi = 0$ at the near side of trigger particles, while at their away side, i.e., around $\Delta\phi = \pi$, there is a broad structure for b = 0 fm but a pronounced peak for b = 8 fm. As shown by dashed lines, the approximate di-hadron azimuthal correlations calculated with Eq. (2) using $\alpha = 1/4$ in determining the event plane (Eq. (3)) reproduce very well the exact ones, and their difference, shown in the lower panels of Fig. 6, is smaller than the residual correlations after subtracting the contributions from anisotropic flows as discussed below.

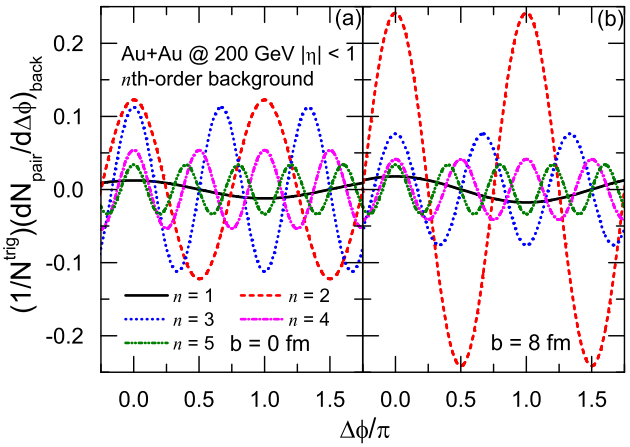


FIG. 7: (Color online) Di-hadron azimuthal correlations per trigger particle from anisotropic flows up to order $n = 5$ in Au+Au collisions at $\sqrt{s_{NN}} = 200$ GeV for impact parameters b = 0 fm (left panel) and b = 8 fm (right panel) from the parameter set B.

As in Ref. [17], we evaluate the contributions to di-hadron azimuthal correlations from anisotropic flows of various orders by replacing the event average of products with the product of event averages in the approximate correlations given in Eq. (2), i.e.,

$$\left(\frac{dN_{\rm pair}}{d\Delta\phi}\right)_{\rm back} = \frac{1}{2\pi}[\langle N^{\rm trig}\rangle_e\langle N^{\rm assoc}\rangle_{\rm e} + 2\sum_{n=1}^{+\infty}\langle N^{\rm trig}v_n^{\rm trig}\rangle_{\rm e}\langle N^{\rm assoc}v_n^{\rm assoc}\rangle_{\rm e}\cos(n\Delta\phi)], \quad (4)$$

where the first term is a constant independent of the azimuthal angle ϕ, and the other terms are the contributions from anisotropic flows. In Fig. 7, we show the di-hadron azimuthal correlations per trigger particle from anisotropic flows up to order $n = 5$. It is seen that the elliptic flow, which has a peak at $\Delta\phi = \pi$, has the largest contribution for b = 8 fm, while for b = 0 fm the contribution from the triangular flow, which has peaks at $\Delta\phi = 2\pi/3$ and $4\pi/3$ in the di-hadron azimuthal correlations, is equally important. Furthermore, the triangular flow is seen to give a larger contribution to the di-hadron azimuthal correlations per trigger particle for b = 0 fm than for b = 8 fm as a result of the larger number of associated particles, although it has a larger value for b = 8 fm than for b = 0 fm as shown in Sec. IV. As to the contributions from higher-order flows v_4 and v_5, they are, on the other hand, relatively small for both b = 0 fm and b = 8 fm.

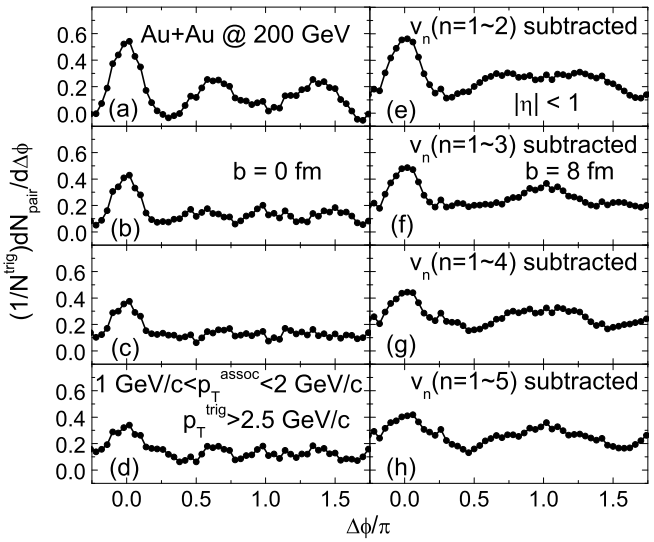


FIG. 8: (Color online) Di-hadron correlations per trigger particle after subtracting background correlations up to different orders in Au+Au collisions at $\sqrt{s_{NN}} = 200$ GeV for b = 0 fm ((a), (b), (c) and (d)) and b = 8 fm ((e), (f), (g) and (h)) from the parameter set B.

The residual di-hadron correlations per trigger particle after subtracting both the constant term in Eq. (4) and the contributions due to anisotropic flows (Fig. 7) from the exact azimuthal correlations (upper panels in Fig. 6) are shown in Fig. 8. It is seen from Figs. 8(a) and (e) that the away-side double-peak structure is much stronger for b = 0 fm than for b = 8 fm after subtracting the contribution from the direct flow as well as the large contribution from the elliptic flow. Subtracting also the contribution from the triangular flow as shown in Figs. 8(b) and (f) changes the away-side double peaks in the di-hadron azimuthal correlations to essentially flat correlations for b = 0 fm but to a single peak for b = 8 fm, while the near-side peak is reduced in both cases. As expected from the small contributions due to higher-order flows shown in Fig. 7, further subtraction of the contributions from higher-order anisotropic flows does not change much the shape of the di-hadron correlations as shown in Figs. 8(c) and (g) as well as in Figs. 8(d) and (h). The residual di-hadron azimuthal correlations per trigger particle af-

ter the subtraction of the contributions from anisotropic flows are then the correlations induced by initially produced back-to-back jet pairs. Our results indicate that the away-side jets essentially disappear in the produced medium in collisions at b = 0 fm but are still visible in collisions at b = 8 fm, consistent with the observed larger jet quenching in central than in mid-central collisions. The away-side double-peak structure in Figs. 8(a) and (e) after subtracting the contribution from the elliptic flow is thus from the combined effects of the away-side jets and the higher-order anisotropic flows, particularly the triangular flow. The weaker away-side double-peak structure for b = 8 fm in Fig. 8 (e) than for b = 0 fm in Fig. 8 (a) then reflects the effect due to the remnant of away-side jets and the relatively smaller contribution per trigger particle from the triangular flow shown in Fig. 7.

It is interesting to compare present results based on the parameter set B with those in Refs. [17] and [31] based on the parameter set A for b = 8 fm and b = 0 fm, respectively. For the case of b = 8 fm, the away-side double-peak structure is weaker for the parameter set B than for the parameter set A, and the reasons for this are similar to those that cause its weakening in comparison to the case of b = 0 fm based on the same parameter set. For the case of b = 0 fm, the conclusion that the away-side double-peak structure in the results from the parameter set B is mainly due to the triangular flow is different from that in Ref. [31] based on the parameter set A, which seems to indicate that other effects such as jet deflections or Mach cone shock waves are also relevant.

VI. SPECIFIC VISCOSITY

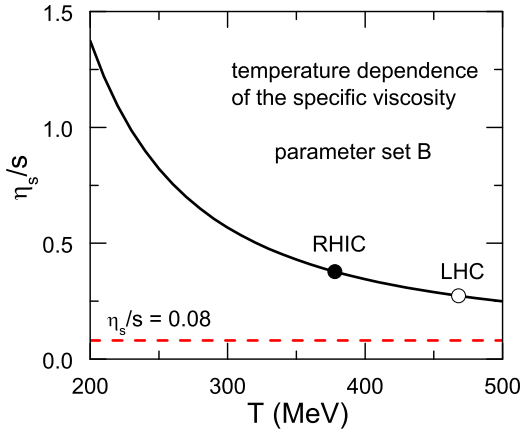


FIG. 9: (Color online) Temperature dependence of the specific viscosity in the partonic matter from the parameter set B.

With the success of the parameter set B in describing measured elliptic flow in heavy ion collisions at both RHIC and LHC, it is of interest to estimate the specific viscosity in the partonic matter formed in these collisions. In the kinetic theory, the shear viscosity is given by $\eta_s = 4\langle p\rangle/(15\sigma_{\rm tr})$ in terms of the parton mean momentum $\langle p\rangle$ and the parton transport or viscosity cross section $\sigma_{\rm tr} = \int dt d\sigma/dt(1-\cos^2\theta)$, where t is the standard Mandelstam variable for four-momentum transfer and $d\sigma/dt \approx 9\pi\alpha_s^2/[2(t-\mu^2)^2]$ is the differential cross section used in the AMPT model. By assuming that the partonic matter only consists of non-interacting massless up and down quarks as in the AMPT model, we have $\langle p\rangle = 3T$ and the entropy density $s = (\epsilon + P)/T = 4\epsilon/(3T) = 96T^3/\pi^2$ with T being the temperature of the partonic matter. The specific viscosity, i.e., the ratio between the shear viscosity and the entropy density, is then [24]

$$\eta_s/s \approx \frac{3\pi}{40\alpha_s^2}\frac{1}{\left(9+\frac{\mu^2}{T^2}\right)\ln\left(\frac{18+\mu^2/T^2}{\mu^2/T^2}\right)-18}. \qquad (5)$$

The temperature dependence of the specific viscosity obtained from the parameter set B is shown in Fig. 9, and it shows that the specific viscosity decreases with increasing temperature. With the energy density of the baryon-free quark and antiquark matter given by $\epsilon = 72T^4/\pi^2$, the initial temperature T is found to be about 378 MeV in Au+Au collisions at $\sqrt{s_{NN}} = 200$ GeV and 468 MeV in Pb+Pb collisions at $\sqrt{s_{NN}} = 2.76$ TeV from the average energy density of mid-rapidity partons at their average formation time [24]. The specific viscosity is then about 0.377 at RHIC energy and 0.273 at LHC energy as indicated, respectively, by the solid and open circles in Fig. 9. The values are thus similar at RHIC and LHC, although both are much larger than the lower bound $\eta_s/s \approx 0.08$ predicted by the AdS/CFT correspondence [34].

VII. SUMMARY

Using the default values for the parameters in the Lund string fragmentation function and a smaller but more isotropic parton scattering cross section than previously used in the AMPT model for heavy ion collisions at RHIC, we have obtained a good description of both the charged particle multiplicity density and the elliptic flow measured in Au+Au collisions at $\sqrt{s_{NN}} = 200$ GeV, although the transverse momentum spectra are still softer than the experimental results. With these constrained parameters, the magnitude of the triangular flow in these collisions has been predicted. We have also studied the di-hadron azimuthal correlations triggered by energetic hadrons at both impact parameters of b = 0 and 8 fm and found that the double-peak structure at the away side of triggered particles, which is seen after subtracting the background contributions due to the elliptic flow, is largely due to the triangular flow. However, the residual correlations shown in our study after the subtraction of the flow contribution might still contain the contribution

from flow fluctuations besides the nonflow contribution that we are interested in [35]. It will be of great interest to find a method that can disentangle the nonflow contribution from that due to flow fluctuations.

We have also estimated the specific viscosity in the initial partonic matter and found that it is much larger than the lower bound predicted by the AdS/CFT correspondence and is thus different from the values extracted with the viscous hydrodynamic model. The different conclusions from the hydrodynamic model and the AMPT model might come from the fact that a constant specific viscosity is used in the former model while a constant total cross section is used in the latter one. Including the temperature dependence of the local screening mass in the evaluation of the parton scattering cross section in the AMPT model as in Ref. [36] may help to better understand the different results from the transport model and the hydrodynamic model.

Acknowledgments

We thank Fuqiang Wang and You Zhou for helpful comments. This work was supported in part by the U.S. National Science Foundation under Grant No. PHY-0758115, the US Department of Energy under Contract No. DE-FG02-10ER41682, and the Welch Foundation under Grant No. A-1358.

[1] I. Arsene *et al.* (BRAHMS Collaboration), Nucl. Phys. **A757**, 1 (2005).
[2] K. Adcox *et al.* (PHENIX Collaboration), Nucl. Phys. **A757**, 184 (2005).
[3] B.B. Back *et al.* (PHOBOS Collaboration), Nucl. Phys. **A757**, 28 (2005).
[4] J. Adams *et al.* (STAR Collaboration), Nucl. Phys. **A757**, 102 (2005).
[5] D. Teaney, J. Lauret, and E.V. Shuryak, Phys. Rev. Lett. **86**, 4783 (2001).
[6] P. Huovinen, P.F. Kolb, and U. Heinz, Nucl. Phys. **A698**, 475 (2002).
[7] T. Hirano and K. Tsuda, Phys. Rev. C **66**, 054905 (2002).
[8] P. Romatschke and U. Romatschke, Phys. Rev. Lett. **99**, 172301 (2007).
[9] Z.W. Lin, C.M. Ko, and S. Pal, Phys. Rev. Lett. **89**, 152301 (2002).
[10] D. Molnar and M. Gyulassy, Nucl. Phys. **A697**, 495 (2002); D. Molnar, Nucl. Phys. **A703**, 893 (2002).
[11] L.W. Chen, C.M. Ko, and Z.W. Lin, Phys. Rev. C **69**, 031901(R) (2004).
[12] P. Sorensen, J. Phys. G **37**, 094011 (2010).
[13] B. Alver and G. Roland, Phys. Rev. C **81**, 054905 (2010).
[14] B.H. Alver, C. Gombeaud, M. Luzum, and J.Y. Ollitrault, Phys. Rev. C **82**, 034913 (2010).
[15] H. Petersen, G.Y. Qin, S.A. Bass, and B. Müller, Phys. Rev. C **82**, 041901 (2010).
[16] B. Schenke, S. Jeon, and C. Gale, Phys. Rev. Lett. **106**, 042301 (2011).
[17] J. Xu and C.M. Ko, Phys. Rev. C **83**, 021903(R) (2011).
[18] Z.W. Lin, C.M. Ko, B.A. Li, B. Zhang, and S. Pal, Phys. Rev. C **72**, 064901 (2005).
[19] X.N. Wang and M. Gyulassy, Phys. Rev. D **44**, 3501 (1991).
[20] B. Zhang, Comp. Phys. Comm. **109**, 193 (1998).
[21] B.A. Li and C.M. Ko, Phys. Rev. C **52**, 2037 (1995).
[22] Z. W. Lin, S. Pal, C.M. Ko, B.A. Li, and B. Zhang, Phys. Rev. C **64**, 011902(R) (2001).
[23] Z.W. Lin and C.M. Ko, Phys. Rev. C **65**, 034904 (2002).
[24] J. Xu and C.M. Ko, Phys. Rev. C **83**, 034904 (2011).
[25] I.G. Bearden *et al.* (BRAHMS Collaboration), Phys. Rev. Lett. **88**, 202301 (2002).
[26] W. Broniowski and W. Florkowski, Phys. Rev. C **65**, 024905 (2002).
[27] S.S. Adler *et al.* (PHENIX Collaboration), Phys. Rev. C **69**, 034910 (2004).
[28] S. Afanasiev *et al.* (PHENIX Collaboration), Phys. Rev. C **80**, 024909 (2009).
[29] S. Wang, Y.Z. Jiang, Y.M. Liu, D. Keane, D. Beavis, S.Y. Chu, S.Y. Fung, M. Vient, C. Hartnack, and H. Stöcker, Phys. Rev. C **44**, 1091 (1991).
[30] N. Borghini, P.M. Dinh and J.Y. Ollitrault, Phys. Rev. C **64**, 054901 (2001).
[31] G.L. Ma and X.N. Wang, Phys. Rev. Lett. **106**, 162301 (2011).
[32] H. Agakishiev *et al.* (STAR Collaboration), arXiv:1010.0690 [nucl-ex].
[33] M. Luzum, Phys. Lett. **B696**, 499 (2011).
[34] P.K. Kovtun, D.T. Son and A.O. Starinets, Phys. Rev. Lett. **94**, 111601 (2005).
[35] L. Yi, F.Q. Wang and A.H. Tang, arXiv:1101.4646 [nucl-th].
[36] B. Zhang and W. A. Wortman, Phys. Lett. **B693**, 24 (2010).